

## Original

Kieke, M.; Feyerabend, F.; Lemaitre, J.; Behrens, P.; Willumeit-Römer, R.:

**Degradation rates and products of pure magnesium exposed to different aqueous media under physiological conditions.**

In: BioNanoMaterials. Vol. 17 (2016) 3-4, 131 - 143.

First published online by de Gruyter: 29.04.2016

<http://dx.doi.org/10.1515/bnm-2015-0020>

## Letter

Marc Kieke<sup>a</sup>, Frank Feyerabend<sup>a,\*</sup>, Jacques Lemaitre, Peter Behrens and Regine Willumeit-Römer

# Degradation rates and products of pure magnesium exposed to different aqueous media under physiological conditions

DOI 10.1515/bnm-2015-0020

Received November 24, 2015; accepted April 1, 2016; previously published online April 29, 2016

**Abstract:** As magnesium and many of its alloys are a promising class of degradable implant materials, a thorough understanding of their degradation under physiological conditions is a key challenge in the field of biomaterial science. In order to increase the predictive power of in vitro studies, it is necessary to imitate the in vivo conditions, track the decomposition process and identify the products that form during the degradation pathway. In this in vitro study, slices of pure magnesium were exposed to Hank's Balanced Salt Solution (HBSS), Dulbecco's Modified Eagle Medium (DMEM) and simulated body fluid (SBF), respectively, under cell culture conditions, which included CO<sub>2</sub> gassing. The series were repeated with supplements of fetal bovine serum (FBS), added to the respective media. Degradation rates, osmolality and pH were found to vary with the choice of medium and supplementation with proteins. In order to identify the crystalline degradation products, the crusts formed on the specimens were investigated via X-ray diffraction (XRD) measurements. As

expected, brucite, Mg(OH)<sub>2</sub>, was found among the degradation products; interestingly, nesquehonite, Mg(HCO<sub>3</sub>)(OH)·2H<sub>2</sub>O, was found to be the dominant degradation product in this study. The experimental data are well in accordance with solubility calculations.

**Keywords:** brucite; Dulbecco's Modified Eagle Medium; Hank's Balanced Salt Solution; nesquehonite; pure magnesium; simulated body fluid.

## Introduction

Magnesium and its alloys have gained increasing interest in the field of temporary implant materials [1]. Biodegradable cardiovascular magnesium stents were successfully tested for clinical applications [2, 3]. Due to its mechanical properties, which are similar to those of bone, magnesium is also of high interest for orthopedic research [4]. Also, metallic magnesium and its degradation product magnesium hydroxide show osteoconductive properties [5, 6].

As magnesium is highly susceptible to degradation in aqueous environments, efforts have been made both to decelerate as well as to exploit this process. For the application as a part of large, load-bearing prosthesis, an uncontrolled, i.e. too rapid, degradation is obviously a major disadvantage. On the other hand, the osteoconductive properties mentioned can support the incorporation of an implant made of or coated with magnesium or magnesium compounds [7, 8]. Thus, the degradation of metallic magnesium is an obstacle as well as an opportunity in the field of degradable biomaterials. A thorough understanding of the kinetics and mechanisms of this process is therefore crucial in order to better evaluate the degradation behavior and in this way increase the predictive power of in vitro studies, the results of which have so far often differed considerably from those of in vivo studies [4, 9]. In vitro degradation setups provide many opportunities to follow the course of decomposition online, such as pH and conductivity monitoring [10, 11],

<sup>a</sup>Marc Kieke and Frank Feyerabend: These authors contributed equally to this study.

**\*Corresponding author: Dr. Frank Feyerabend**, Helmholtz-Zentrum Geesthacht, Institute of Materials Science, Division Metallic Biomaterials, Department for Material Design and Characterization, Max-Planck-Str. 1, 21502 Geesthacht, Germany, Phone: +49 (0)4152 871259, Fax: +49 (0)4152 872595, E-mail: frank.feyerabend@hzg.de, <http://orcid.org/0000-0001-9532-0207>

**Marc Kieke and Peter Behrens:** Institute for Inorganic Chemistry, Leibniz University of Hannover, Callinstr. 9, 30167 Hannover, Germany

**Jacques Lemaitre:** École Polytechnique Fédérale de Lausanne, EPFL STI-DO, MXD 337 (Bâtiment MXD), Station 12, CH-1015 Lausanne, Switzerland

**Regine Willumeit-Römer:** Helmholtz-Zentrum Geesthacht, Institute of Materials Science, Division Metallic Biomaterials, Max-Planck-Str. 1, 21502 Geesthacht, Germany

but the identity of the degradation products formed from magnesium and the supplements of the media cannot be derived from these parameters alone. Electron-dispersive X-ray spectroscopy (EDS) analysis can be performed discontinuously on the degradation products to gain information on their composition, but without providing speciation between different products with the same elemental formula. Moreover, most instruments only give semi-quantitative data, because they are not calibrated to the respective elements. X-ray diffraction (XRD) measurements provide more detailed information at least about the crystalline degradation products.

Magnesium hydroxide is the dominant crystalline degradation product of magnesium and its alloys upon exposure to aqueous media, as has been shown before by various studies [12]. As the solubility of the hardly soluble  $\text{Mg}(\text{OH})_2$  can be increased, for example, by the presence of chloride ions [13, 14] and by buffering of pH, magnesium hydroxide is not the only product which can be expected. Alternative products such as phosphates and carbonates, respectively, were found in various studies. In an *in vivo* approach, a magnesium containing calcium phosphate ( $\text{Mg}_x\text{Ca}_y(\text{PO}_4)_z$ ) was found after the degradation on the surface of a Mg-Mn-Zn alloy [7], while the degradation of a magnesium rare-earth alloy led to the *in vitro* formation of complex products with the general formula  $(\text{Mg},\text{Ca})_x(\text{PO}_4)_y(\text{CO}_3)_z(\text{OH})_l$  [15]. The formation of magnesium carbonates ( $\text{MgCO}_3$ ) was reported by various authors, when pure magnesium was exposed to different aqueous media [16, 17]. However, many studies did not distinguish between different modifications of the carbonates and phosphates, respectively.

With regard to the issues mentioned, it is of central interest to estimate the degradation rates and products of magnesium exposed to aqueous media under conditions similar and relevant to *in vivo* conditions. For this purpose, we have studied the degradation of pure magnesium under cell culture conditions in cell-free media. As the respective media Hank's Buffered Salt Solution (HBSS), simulated body fluid (SBF) and Dulbecco's Modified Eagle Medium (DMEM) were applied. The cell culture conditions included a  $\text{CO}_2$  (5%) and  $\text{O}_2$  (21%) gassing, as well as a temperature of 37 °C and 95% relative humidity over the entire experiment. In an additional set of experiments, fetal bovine serum was added to all the above-mentioned media to include the influence of bioorganic components. Degradation rates were determined by measuring the weight loss of the samples. In order to identify the degradation products, the specimens were investigated by scanning electron microscopy (SEM) and XRD. The latter is suitable for the

identification of crystalline phases that may have formed and have been deposited during the degradation process either directly or by follow-up reactions.

## Materials and methods

### Magnesium casting

A magnesium ingot (purity 99.95 wt.%) was prepared by permanent mold casting. The material was molten under a protective atmosphere ( $\text{Ar}+2\% \text{SF}_6$ ) at a temperature of 750 °C. The melt was stirred for 30 min with 200 rpm prior to casting the material into preheated molds (550 °C) made out of mild steel. To assure cleanliness of the cast ingots, a filter (Foseco SIVEX FC, Foseco GmbH, Borken, Germany) was used. Cylindrical specimens with a diameter of 10 mm and a height of 1.5 mm were cut from the cast blocks via electrical discharge machining. Apart from sterilization the samples were used without further treatment.

### Degradation media

Three different media were used for the degradation tests: (I) HBSS without  $\text{Ca}^{2+}$  and  $\text{Mg}^{2+}$  ions (Life Technologies, Darmstadt, Germany) as a low-buffered solution; (II) DMEM Glutamax-I (Life Technologies, Darmstadt, Germany) as a more complex, highly buffered solution, and (III) SBF (SBF-JL2, according to [18]). For the preparation of the SBF two solutions were prepared. All chemicals were obtained from Merck (Darmstadt, Germany). (I) Solution A: 6.129 g NaCl, 5.89 g  $\text{NaHCO}_3$  and 0.498 g  $\text{Na}_2\text{HPO}_4 \cdot 2\text{H}_2\text{O}$  were dissolved in 1 L of double-distilled water. After dissolution, 0.934 mL of 1 M HCl was added. (II) Solution B: 6.129 g NaCl and 0.54 g  $\text{CaCl}_2$  were dissolved in 1 L double-distilled water and 0.934 mL of 1 M HCl was added. Both solutions were kept separately in the fridge and mixed (1:1) directly before the experiment. The pH value of the resulting solution was 7.4. A comparison of the compositions is given in Table 1. In a second set of experiments, 10% or 20% FBS (FBS, PAA Laboratories, Linz, Austria) were added to these media.

### Determination of degradation rate, pH and osmolality

The degradation rate was determined by weight loss. Each sample was weighed (Scaltec SBA52, Scaltec Instruments GmbH, Göttingen, Germany) and sterilized (20 min in ultrasonic bath with 70% ethanol) prior to the immersion ( $n=6$  per solution). After 3 days of incubation under cell culture conditions the samples were taken from the different media and dried at 37 °C under vacuum overnight. Degradation residues from the samples were removed by immersion in chromic acid (180 g/L in distilled water, VWR International, Darmstadt, Germany). The immersion was carried out two times for 10 min, with the samples being turned over in between. Afterwards the samples were rinsed in distilled water and 100% ethanol. After drying, the weight of the samples was measured again and the degradation rate (DR) was calculated according to equation 1 [19].

**Table 1:** Compositions of the used corrosion media.

Ingredient	HBSS		DMEM		SBF	
	mg/L	mM	mg/L	mM	mg/L	mM
Amino acids			1852	10.29		
Vitamins			31.6	0.15		
Inorganic salts						
Calcium chloride ( $\text{CaCl}_2 \cdot 2\text{H}_2\text{O}$ )			264	1.80	270	1.84
Ferric nitrate ( $\text{Fe}(\text{NO}_3)_3 \cdot 9\text{H}_2\text{O}$ )			0.1	0.000248		
Hydrochloric acid (HCl)					934	0.934
Magnesium sulfate ( $\text{MgSO}_4 \cdot 7\text{H}_2\text{O}$ )			200	0.813		
Potassium chloride (KCl)	400	5.37	400	5.37		
Potassium phosphate monobasic ( $\text{KH}_2\text{PO}_4$ )	60	0.44				
Sodium bicarbonate ( $\text{NaHCO}_3$ )	350	4.17	3700	44.04	2945	35.06
Sodium chloride (NaCl)	8000	136.98	6400	109.51	6129	104.88
Sodium phosphate monobasic ( $\text{NaH}_2\text{PO}_4 \cdot 2\text{H}_2\text{O}$ )			141	0.9		
Sodium phosphate dibasic ( $\text{Na}_2\text{HPO}_4$ ) anhydrous	48	0.34			249	1.75
Other components						
D-Glucose (dextrose)	1000	5.56	4500	25.00		
Phenol red			15	0.0399		
Sodium pyruvate			110	1.000		

$$\text{DR} = \frac{8.76 \cdot 10^4 \cdot \Delta W}{A \cdot t \cdot \rho} \quad (1)$$

where  $A$  is the surface area in  $\text{cm}^2$ ,  $t$  is the time in hours,  $\rho$  is the density of pure Mg ( $1.74 \text{ g/cm}^3$ ) and  $\Delta W$  is the observed mass loss in g.

After the immersion of the specimens the different media were removed from the wells and used for analysis of the pH value and osmolality. Solutions without samples were incubated in parallel as controls. The pH value was measured by a standard laboratory pH meter (Sentron SI600, Sentron Europe BV, Roden, The Netherlands) with an ISFET electrode. The osmolality of the supernatants was analyzed by a cryoscopic osmometer (Osmomat Auto, Gonotec GmbH, Berlin, Germany). Fifty microliters of the supernatant were used for the measurement. The device is a freezing point osmometer which determines the osmolality by measuring the freezing point. This decreases by  $1.86^\circ\text{C}$  when 1 mole of a nonionic solute is added to 1 kg of solvent [20].

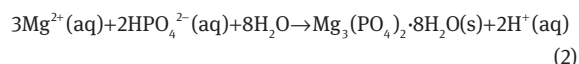
## Identification of degradation products

**Immersion procedure:** Pure magnesium samples were sonicated for 20 min in dry isopropanol, dried and gamma-sterilized at the in core irradiation (ICI) facility of the Geestacht Neutron Facility with a total dosage of 29 kGy. All specimens were immersed under sterile conditions in 1 mL (solid/liquid ratio of 0.2 g/mL) of the respective media in agarose-coated 12-well plates (Greiner Bio-One, Frickenhausen, Germany). Then the samples were incubated under cell culture conditions ( $37^\circ\text{C}$ , 5%  $\text{CO}_2$ , 21%  $\text{O}_2$  and 95% relative humidity) in an incubator (Heraeus BBD 6620, Fisher Scientific, Schwerte, Germany). The immersion time was 1, 2, 3, 4 and 7 days, respectively. Neither a pH adjustment nor a liquid stream was applied. After the immersion all samples were rinsed with deionized water for 1 min, dried under vacuum and stored at room temperature. Immersion experiments were performed in duplicate.

**Characterization:** The samples were visualized using a scanning electron microscope (SEM; Auriga, Zeiss, Oberkochen, Germany) to visualize the degradation layers. Images were taken at an accelerating voltage of 20 keV with the secondary electron detector (SE2). In order to identify the crystalline products formed and deposited, XRD measurements were performed on a Stoe Theta/Theta diffractometer (Stoe, Darmstadt, Germany) in reflection mode using  $\text{Cu K}\alpha$  radiation ( $\lambda = 1.54060 \text{ \AA}$ ). The  $2\theta$  range was scanned applying a step size of  $0.01^\circ$  (3.0 s per step). The diffractometer was operated at 40 kV and 30 mA. No further sample preparations were made for the XRD measurements. All samples were placed flatly in a sample holder and adjusted to the X-ray beam.

**Thermodynamical solubility calculations:** Additionally to the formation of brucite and magnesite in HBSS some other degradation products can form. Besides  $\text{Mg}^{2+}$  and carbonates, SBF and cell culture media may contain various ions, including  $\text{Na}^+$ ,  $\text{K}^+$ ,  $\text{Ca}^{2+}$ ,  $\text{Cl}^-$ , phosphate and sulfate ions. In standard incubation conditions [temperature  $T = 37^\circ\text{C}$ , partial  $\text{CO}_2$  pressure  $p(\text{CO}_2) = 5.0\%$ , pH close to 7.5], the dominating carbonate and phosphate soluble species are  $\text{HCO}_3^-$  and  $\text{HPO}_4^{2-}$ , respectively. In SBF and culture media containing  $\text{Ca}^{2+}$  and phosphate ions, the following precipitation reactions should also be considered:

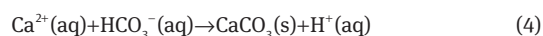
1. Precipitation of magnesium phosphate ( $\text{Mg}_3(\text{PO}_4)_2 \cdot 8\text{H}_2\text{O}$ , bobierite):



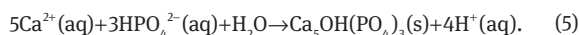
2. Precipitation of calcium hydroxide ( $\text{Ca}(\text{OH})_2$ , portlandite):



3. Precipitation of calcium carbonate ( $\text{CaCO}_3$ , calcite):

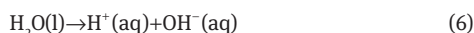


4. Precipitation of calcium phosphate ( $\text{Ca}_5\text{OH}(\text{PO}_4)_3$ , hydroxyapatite):

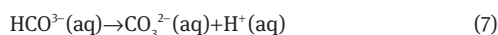


Some other reactions taking place in aqueous solutions deserve to be mentioned.

Dissociation of water ( $\text{pK}^\circ$  (37 °C)=13.61):



Dissociation of hydrogen carbonate ions ( $\text{pK}^\circ$  (37 °C)=10.24):



Dissociation of hydrogen phosphate ions ( $\text{pK}^\circ$  (37 °C)=12.32):

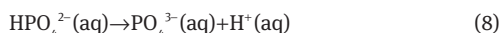


Table 2 presents the equilibrium dissolution constants at 37 °C for the precipitates considered in the present study ( $\text{pK} = -\log_{10} K$ ). Tables 1 and 3 summarize the compositions and main physico-chemical

parameters of the incubating solutions considered in the present study. The saturation index  $S^\circ(X)$  is given by:

$$S^\circ(X) = \log \frac{\Pi(X)}{K(X)} \quad (9)$$

where  $\Pi(X)$  is the ionic product of the ions released upon dissolution of precipitate  $X$ , and  $K(X)$  the equilibrium constant of the dissolution reaction; for instance, in the case of brucite:

$$S^\circ(\text{Brucite}) = \log \frac{(\text{Mg}^{2+})(\text{OH}^-)^2}{K(\text{Brucite})}; \quad K(\text{Brucite}) = (\text{Mg}^{2+})_{\text{Sat}} (\text{OH}^-)_{\text{Sat}}^2. \quad (10)$$

A positive  $S^\circ(X)$  means that the solution is supersaturated in  $X$ , so that the precipitation of  $X$  is thermodynamically possible. However, the actual formation of a precipitate  $X$  depends on the kinetics of nucleation and growth of  $X$  crystals: if the kinetic process is inhibited for some reason (e.g. large free energy of nucleation), the solution can remain in a metastable state without precipitate formation.

## Statistics

Data are displayed as mean  $\pm$  standard deviation (SD). Statistical analysis was performed by using the SigmaStat Software (Systat GmbH, Erkrath, Germany; version 11.0). Comparison of degradation rates was analyzed by applying the one-way analysis of variance (ANOVA) with Holm-Sidak post-hoc test. The significance level was  $p < 0.05$ .

## Editing of figures

All figures were finished with PowerPoint (Microsoft Office 2007 and 2010). Raw figure material was created and edited, respectively, using: SigmaPlot (Version 11, Systat Software Inc.) for Figures 5 and 6; Origin (OriginLab) for Figures 7–9; PowerPoint (Microsoft Office 2007 and 2010) for Figure 10.

# Results

## Morphological analysis

All samples showed obvious signs of degradation on the surface. Exemplary photographs of samples are given in Figures 1–3. Figure 1 shows the surfaces of samples immersed in HBSS medium and in HBSS supplemented with 10% FBS, Figure 2 shows corresponding photographs for samples from DMEM and the corresponding 10% FBS-supplemented medium, and Figure 3 for the samples from SBF-based media. In general, the amount of white crust and flakes fallen off from the samples, respectively, increased with immersion time; however, the exact time points of the chipping off were not determined. According to the appearances, degradation occurred fastest in HBSS.

**Table 2:** Dissolution constants of selected precipitates.

Precipitate	Dissolution reaction	pK (37 °C)
Brucite	$\text{Mg}(\text{OH})_2 \rightarrow \text{Mg}^{2+} + 2\text{OH}^-$	11.25
Magnesite	$\text{MgCO}_3 \rightarrow \text{Mg}^{2+} + \text{CO}_3^{2-}$	5.51
Nesquehonite	$\text{Mg}(\text{HCO}_3)_2 \cdot 2\text{H}_2\text{O} \rightarrow \text{Mg}^{2+} + \text{CO}_3^{2-} + 3\text{H}_2\text{O}$	4.49
Bobierite	$\text{Mg}_3(\text{PO}_4)_2 \cdot 8\text{H}_2\text{O} \rightarrow 3\text{Mg}^{2+} + 2\text{PO}_4^{3-} + 8\text{H}_2\text{O}$	27.62
Portlandite	$\text{Ca}(\text{OH})_2 \rightarrow \text{Ca}^{2+} + 2\text{OH}^-$	5.38
Calcite	$\text{CaCO}_3 \rightarrow \text{Ca}^{2+} + \text{CO}_3^{2-}$	8.44
Hydroxyapatite	$\text{Ca}_5(\text{PO}_4)_3(\text{OH}) \rightarrow 5\text{Ca}^{2+} + 3\text{PO}_4^{3-} + \text{OH}^-$	58.77

**Table 3:** Physico-chemical characteristics of incubating solutions.

	Component	HBSS	SBF	DMEM
Initial				
$S^\circ(X)$	pH	6.69	7.61	7.70
	Brucite	−5.00	−4.41	−1.38
	Nesquehonite	−7.00	−6.11	−1.57
	Calcite	−5.05	0.47	0.55
	Hydroxyapatite	−4.40	1.29	1.21
	Bobierite	−5.81	−5.27	−0.02
Saturated in brucite				
$S^\circ(X)$	pH	8.63	8.64	8.64
	Nesquehonite	0.50	0.50	0.50
	Calcite	−3.47	1.17	1.16
	Hydroxyapatite	−4.25	0.99	0.92
	Bobierite	1.27	1.38	1.29
Saturated in nesquehonite				
$S^\circ(X)$	pH	8.28	8.31	8.31
	Brucite	−0.34	−0.34	−0.34
	Calcite	−3.64	1.01	1.01
	Hydroxyapatite	−4.07	1.18	1.11
	Bobierite	1.11	1.21	1.13

DMEM also contains  $2.5 \times 10^{-4}$  mM  $\text{Fe}(\text{NO}_3)_3$ , not considered in the thermodynamic calculations.



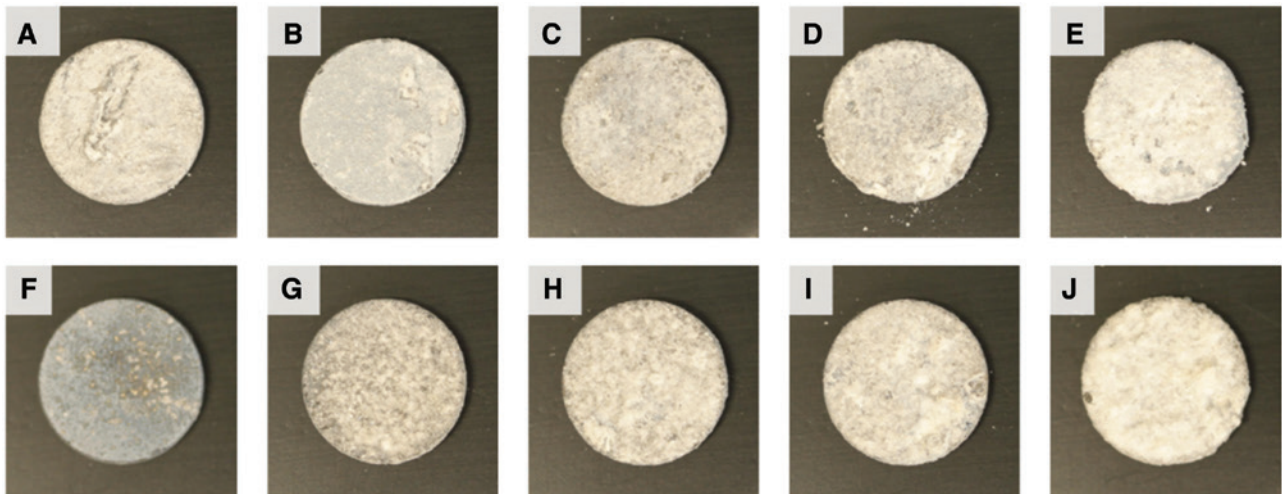


**Figure 1:** Photographs of the samples immersed in (A–E) HBSS and (F–J) HBSS +10% FBS for 1, 2, 3, 4 and 7 days, respectively, from left to right.

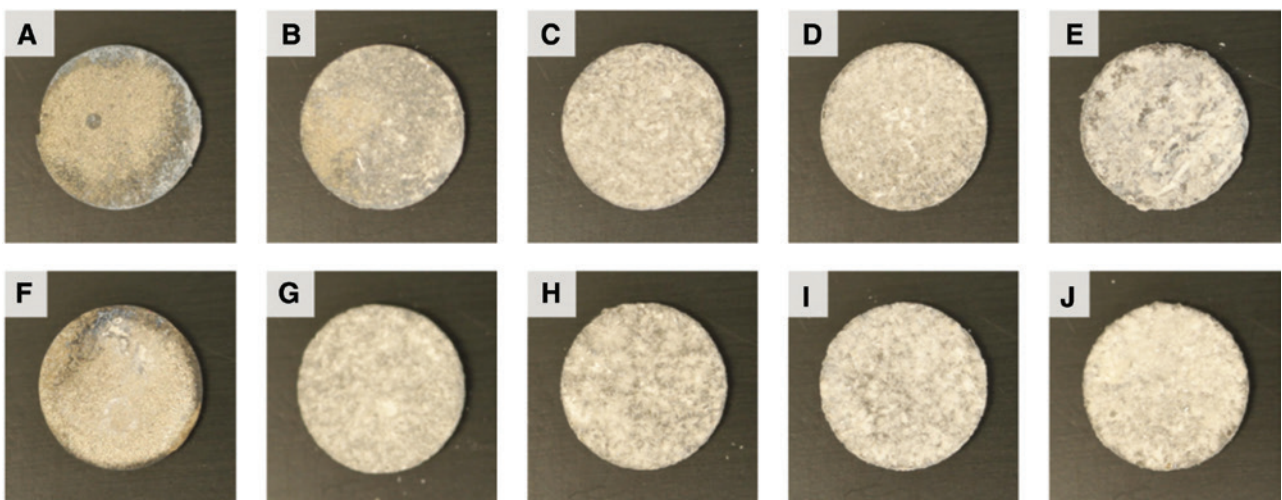


**Figure 2:** Photographs of the samples immersed in (A–E) DMEM and (F–J) DMEM +10% FBS for 1, 2, 3, 4 and 7 days, respectively, from left to right.

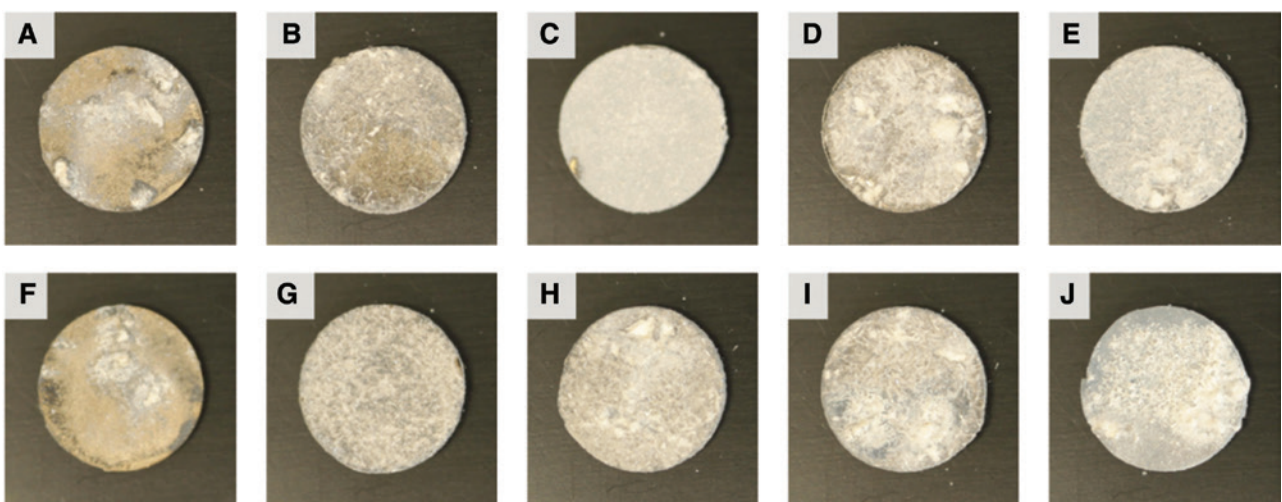


**Figure 3:** Photographs of the samples immersed in (A–E) SBF and (F–J) SBF +10% FBS for 1, 2, 3, 4 and 7 days, respectively, from left to right.

When FBS was supplemented to HBSS and DMEM, degradation seemed to be reduced. In contrast, degradation did apparently not decrease when FBS was supplemented to SBF.

In general, according to the SEM images, two types of crystals with different morphologies predominate within the layer of degradation products (Figure 4). Firstly, intergrown needles, and secondly, crystals with a flake-like shape. However, SEM images from samples which were immersed in different media showed differences between the surface morphologies. Samples immersed in HBSS exhibited mostly flake-like crystals, whereas on

DMEM-immersed samples mainly interconnected needles were visible. In all cases, the appearance of the degradation layer changed with the addition of proteins.

### Degradation rate, pH and osmolality

The degradation rate was highest in HBSS and lowest in SBF. According to the statistical analysis, the HBSS treatment led to significantly higher degradation rates (compared to all other treatments, Figure 5). The actual degradation rates are compared in Figure 6, Top. Using

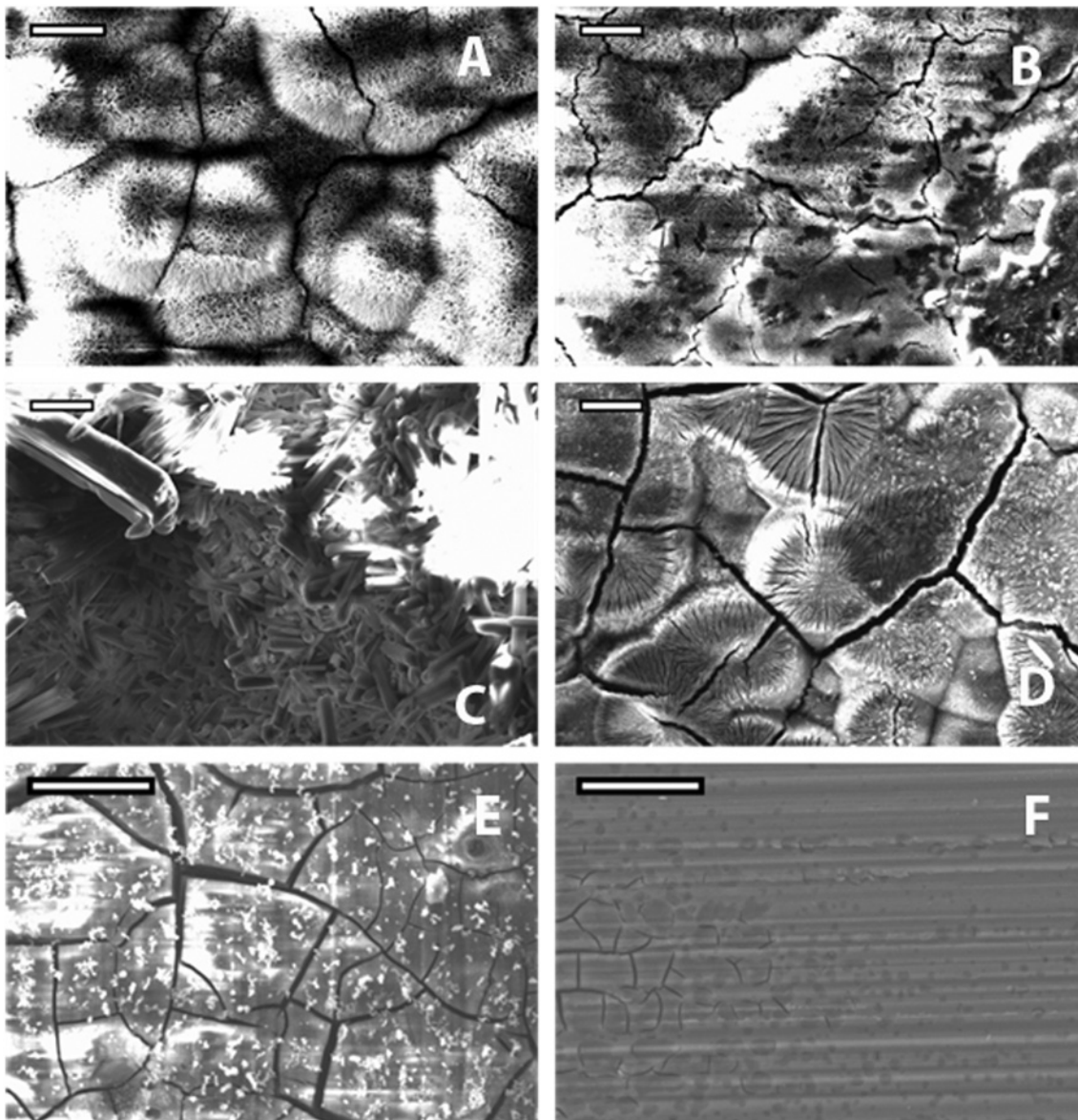


**Figure 4:** SEM images of samples immersed for 72 h in the respective media.

Left column: without FBS supplementation; right column: with FBS supplementation. HBSS (A+B); DMEM (C+D); SBF (E+F). Scale bars represent 25  $\mu\text{m}$ .



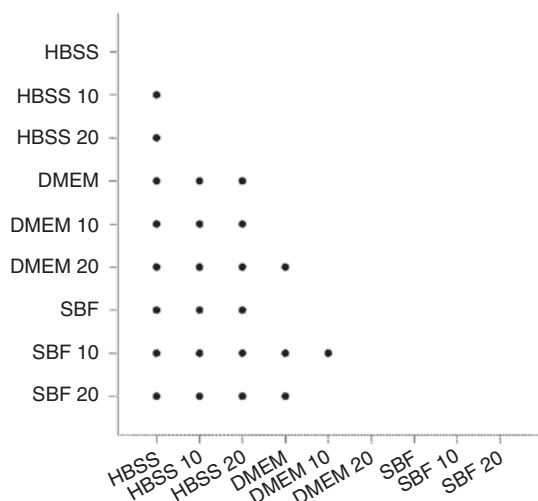


**Figure 5:** Multiple comparison graph of significant differences between the degradation rates in the different solutions (ANOVA,  $p < 0.05$ ). Numbers behind the media designations (HBSS, DMEM, SBF) represent the amount of added FBS (10% or 20%, respectively).

HBSS the addition of proteins exhibited a significant decrease of the degradation rate due to the addition of proteins. This effect was weaker for DMEM, where only the addition of 20% FBS led to a significant decrease. Presumably, due to the low amount of samples, other differences between the degradation rates in DMEM and SBF were not statistically significant. The addition of proteins generally resulted in a decrease of the degradation rate, except for SBF, where the higher amount of protein increased the degradation rate again. The measurement of osmolality reproduces this behavior in the case of DMEM and SBF, but shows a different trend for HBSS (Figure 6 middle). The increase in pH (Figure 6 bottom) appears to show a loose correlation to the degradation rate, when the pH increases as well as the degradation rates in HBSS-based media are both higher. DMEM- and SBF-based media have a higher buffering capacity than HBSS, correspondingly a weaker pH increase is observed; degradation rates are generally smaller as those in HBSS-based media, as well.

## Phase identification via XRD

X-ray diffraction (XRD) investigations allow the qualitative identification (speciation) of different crystalline degradation products. Beforehand, it has to be pointed out that a quantitative evaluation of the species by XRD is not the aim in the present study. Even if this is in principle possible using elaborated standardization and calibration experiments, it does not make sense regarding the way

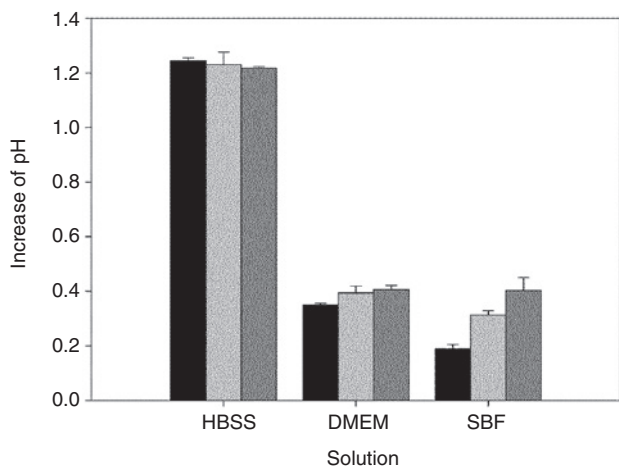
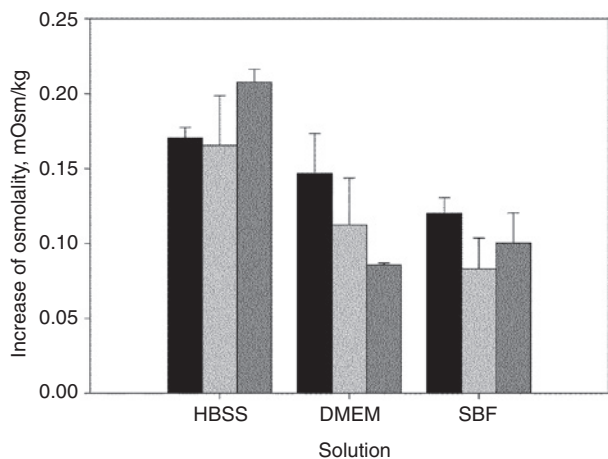
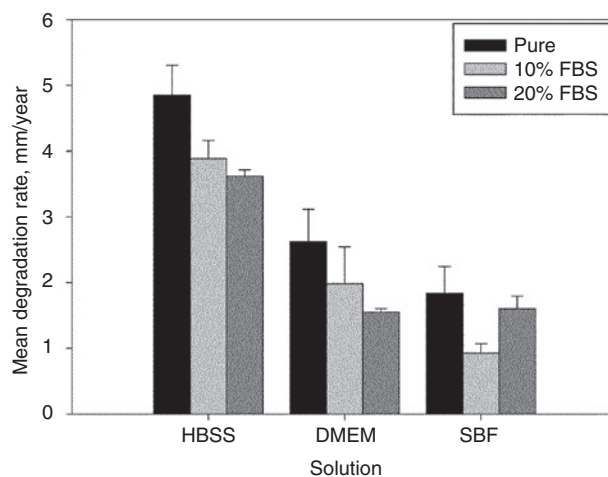


**Figure 6:** Mean degradation rate, increase of osmolality and increase of pH in the different media after immersion of magnesium discs for 72 h.

the samples were produced. Crumbles of different sizes fell off from most samples at undetermined time points. Possible texture effects, which are likely to occur with surface-crystallized or deposited material, would further complicate a quantitative evaluation. Also, reflections



that can be qualitatively assigned to brucite ( $\text{Mg}(\text{OH})_2$ ) or to the substrate magnesium could in some cases hardly be distinguished from background noise.

Exemplary XRD patterns of samples immersed in HBSS or in HBSS supplemented with 10% FBS are shown in Figure 7A; Figure 7B and C show diffractograms for samples immersed in corresponding DMEM- and SBF-based media, respectively.

Reflections associated with metallic magnesium ( $2\theta=32.2^\circ$ ,  $34.4^\circ$  and  $36.6^\circ$ ) were present in all diffractograms, allowing the conclusion that the penetration depth of the X-ray beam was sufficient to examine the crusts in their entire thickness. However, the relative intensities were remarkably low in the DMEM series. For clarity, in the figures the reflections ascribed to magnesium are marked only in the patterns obtained from samples with an immersion time of 1 day. Reflections ascribed to degradation products are marked, if appropriate, in all respective patterns. Brucite,  $\text{Mg}(\text{OH})_2$ , a degradation product observed in many degradation processes of magnesium and magnesium alloys, was in our study only found as one of the products on samples from HBSS-based media (corresponding reflections at  $2\theta=18.5^\circ$  and  $38.0^\circ$ ). Nesquehonite, a magnesium hydroxycarbonate hydroxide hydrate of formula  $\text{Mg}(\text{HCO}_3)(\text{OH})\cdot 2\text{H}_2\text{O}$  (with characteristic reflections at  $2\theta=13.6^\circ$ ,  $23.0^\circ$ ,  $29.5^\circ$  and  $34.2^\circ$ ), was the dominant degradation product in our study. It was observed in all diffractograms from samples from HBSS-based media, and in all diffractograms of specimens that had been exposed to SBF- and DMEM-based media for longer than 1 day. Calcium phosphates were found on a sample immersed in SBF supplemented with 10% FBS for 7 days (Figure 7C). The reflections can be assigned to  $\text{Ca}_2\text{P}_4\text{O}_{12}\cdot 4\text{H}_2\text{O}$  and  $\text{Ca}_2\text{P}_2\text{O}_7\cdot 2\text{H}_2\text{O}$ . However, some reflections, e.g. at  $2\theta=10.2^\circ$  and  $11.6^\circ$ , remained unassigned.

## Discussion

### Influence of the medium and proteins on the degradation rates and osmolality

HBSS has been evaluated to be the simplest medium, followed by SBF, while DMEM also includes organic substances [17]. Degradation rates decreased in the order of HBSS – DMEM – SBF. As proteins are known to retard magnesium degradation under certain conditions [16], a reduction of the decomposition rate was expected for DMEM. The expectation was confirmed for samples immersed in HBSS and DMEM, but not for samples immersed in SBF.

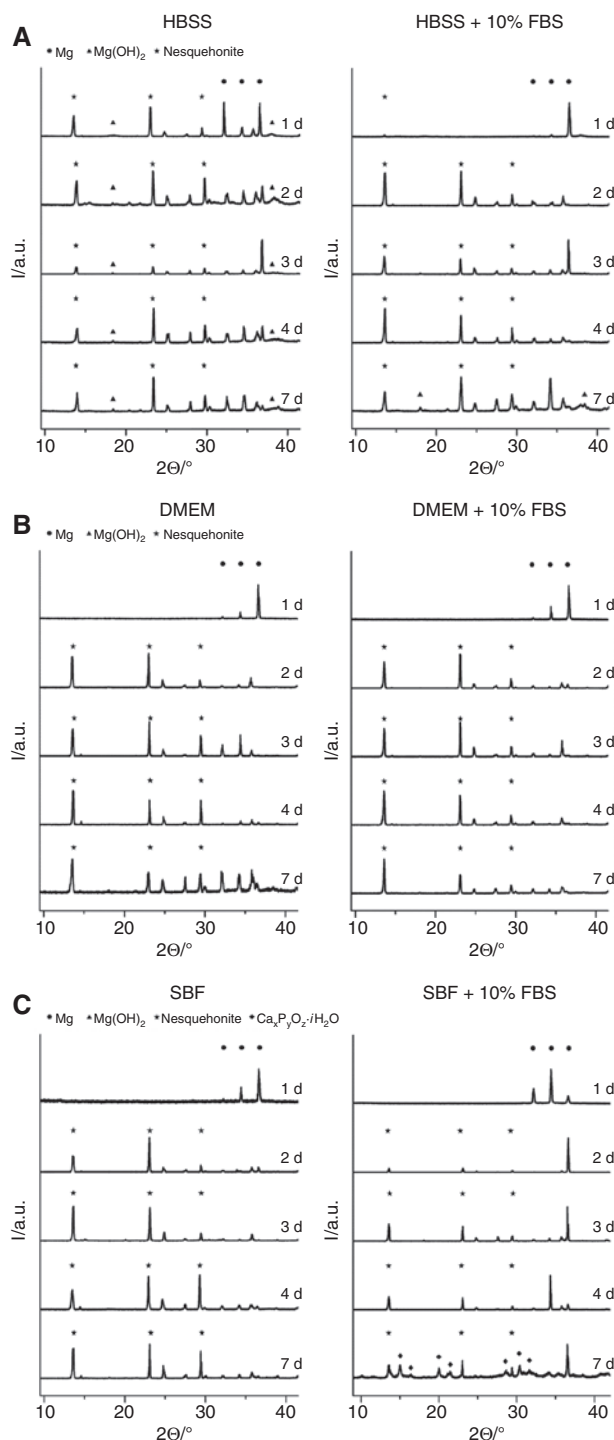


**Figure 7:** XRD patterns obtained from samples immersed without proteins (left) and with proteins (right) in the respective solutions. From top to bottom: 1, 2, 3, 4 and 7 days of immersion. Reflection positions for Mg are indicated in the top patterns, those for  $\text{Mg}(\text{OH})_2$  and nesquehonite in each pattern (if they are present).

As stated above, osmolality examinations reproduced this behavior for DMEM and SBF, but not for HBSS. Presumably due to the high degradation rates in HBSS, which were

the highest in this study, and due to the high salt content of the solutions, a simple correlation could not be found.

## Degradation products

Two magnesium compounds were found to be the dominant degradation products in this study:  $\text{Mg}(\text{OH})_2$  and nesquehonite ( $\text{Mg}(\text{HCO}_3)(\text{OH}) \cdot 2\text{H}_2\text{O}$ ). The latter was found on samples from all media, while  $\text{Mg}(\text{OH})_2$  was found exclusively for specimens which had been exposed to HBSS. Measurements revealed the highest pH when HBSS was used as the medium, hence, the presence of  $\text{Mg}(\text{OH})_2$  in the crusts is plausible. Unfortunately, as described above, the XRD investigations in this study were not suited to be used for quantification. The detection of nesquehonite is in line with the observation of needle-like crystals in SEM images, as this is a typical morphology for this magnesium compound.

In various previous studies,  $\text{Mg}(\text{OH})_2$  has been described as the only crystalline degradation product. However, these studies did not include  $\text{CO}_2$  gassing as part of their setup [12]. Therefore, we ascribe the formation of nesquehonite to the introduction of  $\text{CO}_2$  in our experiments, as carbon dioxide will serve as an additional source of hydrogen carbonate and carbonate ions. In this context, it is of interest that the formation of magnesium carbonates is of relevance for  $\text{CO}_2$  storage using mineral carbonation [21]. The family of magnesium carbonates consists of a variety of compounds, and in other studies with slightly changed parameters in the immersion experiment setups, other members of this family might be formed. Nesquehonite, can be directly synthesized by the addition of a  $\text{NaCO}_3$  solution to a  $\text{MgCl}_2$  solution at room temperature [22]. At slightly elevated temperatures, the  $\text{NaCO}_3$ - $\text{MgCl}_2$  system leads to the formation of hydromagnesite ( $\text{Mg}_5(\text{CO}_3)_4(\text{OH})_2 \cdot 4\text{H}_2\text{O}$ ) [23]. Furthermore, the transformation of nesquehonite to hydromagnesite was reported in the context of dypingite ( $\text{Mg}_5(\text{CO}_3)_4(\text{OH})_2 \cdot 5\text{H}_2\text{O}$ ) [24, 25], which was also found as a byproduct in the synthesis of magnesite ( $\text{MgCO}_3$ ) [26]. Hydromagnesite and magnesite, respectively, were occasionally found to be associated with dolomite (South Australia) [27]. It should be noted that some formulae only differ in one equivalent of crystal water, a difference that in some cases semi-quantitative methods are probably not able to detect reliably, and the formulae of dypingite and giorgiosite are the same ( $\text{Mg}_5(\text{CO}_3)_4(\text{OH})_2 \cdot 5\text{H}_2\text{O}$ ).

The formation of calcium phosphates on samples from the SBF immersion can be traced back to the composition of this medium, which corresponds to a

supersaturated calcium phosphate system. Reflections of crystalline magnesium phosphates were not detected in this study. However, by the characterization methods applied, it cannot be excluded that certain amounts of  $\text{Ca}^{2+}$  were replaced with  $\text{Mg}^{2+}$ . The formation of the calcium phosphates could also be responsible for the small degradation rate of Mg in SBF, as calcium phosphates are a well-known means to stabilize magnesium against too fast degradation [28].

## Probability of degradation products determined by thermodynamical solubility calculations

### HBSS

This solution (HBSS), besides NaCl, also contains KCl,  $\text{NaHCO}_3$ ,  $\text{KH}_2\text{PO}_4$  and  $\text{Na}_2\text{HPO}_4$ ; the latter two components are included as pH buffering additives. The presence of phosphate ions makes possible the precipitation of bobierite. During the increase in Mg concentration resulting from the corrosion process, the pH increases from 6.69 up to 8.63, where the solution is saturated in brucite; at this point, the solution is supersaturated in nesquehonite ( $S^\circ(\text{MC-n})=0.50$ ) and in bobierite ( $S^\circ(\text{TMPO})=1.27$ ) (Figure 8). At saturation in nesquehonite, a lower pH of 8.28 is reached, the solution being then undersaturated in brucite ( $S^\circ(\text{MH})=-0.34$ ), but still supersaturated in bobierite ( $S^\circ(\text{TMPO})=1.11$ ) (Figure 9). Although magnesite is less soluble than nesquehonite (Table 2), it is not observed experimentally. This suggests that, in the present reaction conditions, the nucleation and growth of nesquehonite is favored over that of magnesite. Likewise, the absence of experimentally observed bobierite suggests that its spontaneous nucleation is inhibited in the present experimental conditions.

### SBF

The solution, besides NaCl, also contains  $\text{CaCl}_2$ ,  $\text{NaHCO}_3$  and  $\text{Na}_2\text{HPO}_4$ ; pH buffering is obtained by the presence of carbonates under  $p(\text{CO}_2)=5\%$ . The simultaneous presence of  $\text{Ca}^{2+}$  and  $\text{HPO}_4^{2-}$  in the solution makes possible the precipitation of calcite, hydroxyapatite and bobierite, which show positive initial values of  $S^\circ(X)$  (Table 3). However, long lasting experience has shown that SBF solutions are metastable and can be kept for several weeks without any noticeable precipitation, probably due to the absence of spontaneous nucleation in the bulk of the solution.

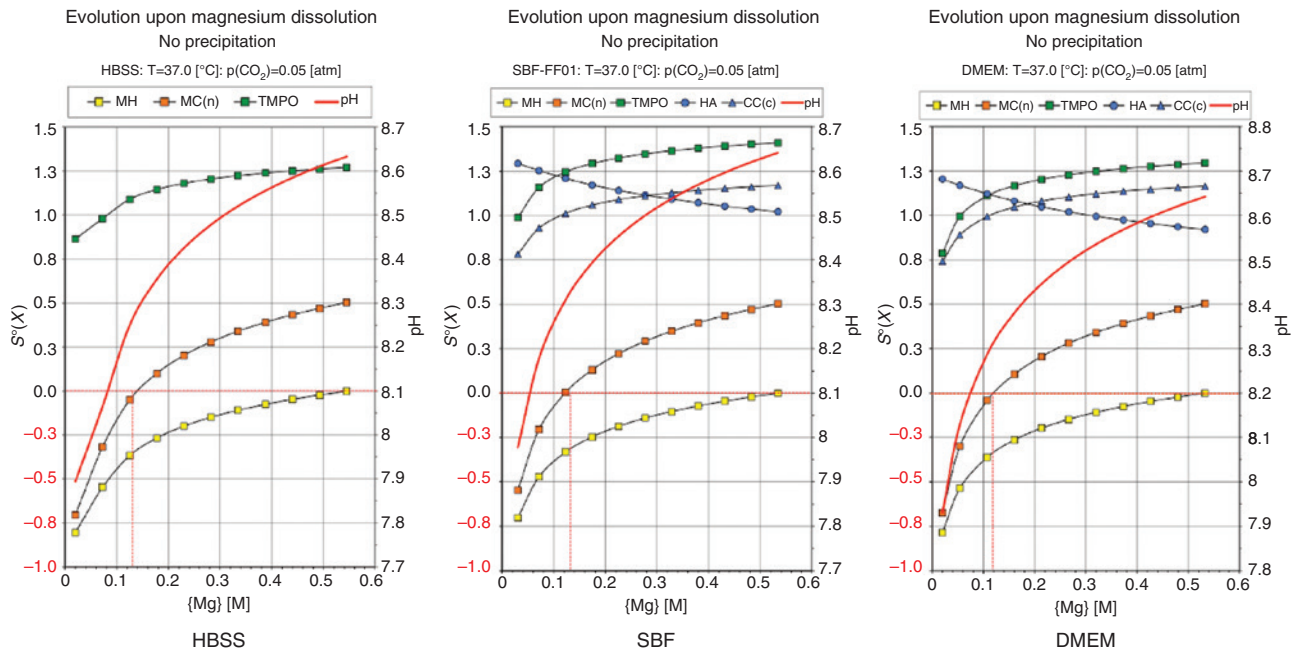


**Figure 8:** Calculation of the saturation index of various compounds without assuming precipitation.

Evolution vs. dissolved Mg of pH and of the standard supersaturations  $S^\circ(X)$  of selected precipitates: MH=brucite- $\text{Mg}(\text{OH})_2$ ; MC(n)=nesquehonite- $\text{MgCO}_3 \cdot 3\text{H}_2\text{O}$ ; TMPO=bobierrite- $\text{Mg}_3(\text{PO}_4)_2 \cdot 8\text{H}_2\text{O}$ ; HA=hydroxylapatite- $\text{Ca}_5\text{OH}(\text{PO}_4)_3$ ; CC(c)=calcite- $\text{CaCO}_3$ . Increase in Mg concentration up to brucite saturation.

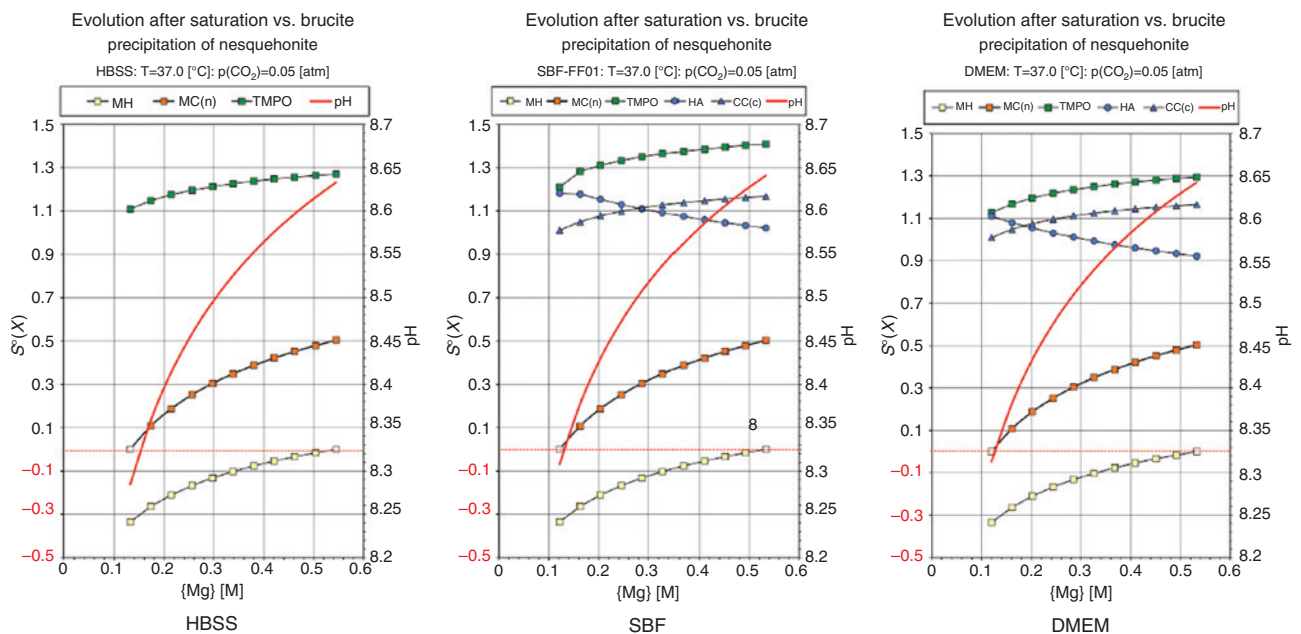


**Figure 9:** Calculation of the saturation index of various compounds related to nesquehonite precipitation.

Evolution vs. dissolved Mg of pH and of the standard supersaturations  $S^\circ(X)$  of selected precipitates: MH=brucite- $\text{Mg}(\text{OH})_2$ ; MC(n)=nesquehonite- $\text{MgCO}_3 \cdot 3\text{H}_2\text{O}$ ; TMPO=bobierrite- $\text{Mg}_3(\text{PO}_4)_2 \cdot 8\text{H}_2\text{O}$ ; HA=hydroxylapatite- $\text{Ca}_5\text{OH}(\text{PO}_4)_3$ ; CC(c)=calcite- $\text{CaCO}_3$ . Decrease in Mg concentration from brucite saturated solutions down to nesquehonite equilibrium.

Only artificial nucleation, for instance in the presence of “bioactive” surfaces can trigger the formation of calcite or hydroxyapatite [18]. The absence of bobierrite found in the present study also suggests that the nucleation of

this precipitate is inhibited just like that of hydroxyapatite. During the increase in Mg concentration resulting from the corrosion process, the pH increases from 7.61 up to 8.64, where the solution is saturated in brucite; at

this point, the solution is supersaturated in nesquehonite ( $S^\circ(\text{MC-n})=0.50$ ), in calcite ( $S^\circ(\text{CC})=1.17$ ), in hydroxyapatite ( $S^\circ(\text{HA})=0.99$ ) and in bobierite ( $S^\circ(\text{TMPO})=1.38$ ) (Figure 8). At saturation in nesquehonite, a lower pH of 8.31 is reached, the solution being then undersaturated in brucite ( $S^\circ(\text{MH})=-0.34$ ), but still supersaturated in calcite ( $S^\circ(\text{CC})=1.01$ ), hydroxyapatite ( $S^\circ(\text{HA})=1.18$ ) and bobierite ( $S^\circ(\text{TMPO})=1.21$ ) (Figure 9). Also in this case the formation of nesquehonite seems to be favored over magnesite. The observation, that calcium phosphates were only observed after 7 days' immersion and in presence of 10% FBS shows that the presence of proteins may be one of the important factors under these experimental conditions.

### DMEM

Medium has an inorganic composition close to that of SBF (Table 1) but also contains many organics (e.g. glucose, amino-acids). The present thermodynamic calculations only simulate the behavior of DMEM solutions free of any organic additives. As for SBF the precipitation of calcite, hydroxyapatite and bobierite is thermodynamically possible, since they show positive initial values of  $S^\circ(X)$  (Table 3). As for SBF solutions, DMEM media seem to be metastable and can be stored for several weeks without any noticeable precipitation. During the increase in Mg concentration resulting from the corrosion process, the pH increases from 7.70 up to 8.64, where the solution is saturated in brucite; at this point, the solution is supersaturated in nesquehonite ( $S^\circ(\text{MC-n})=0.50$ ), in calcite ( $S^\circ(\text{CC})=1.16$ ), hydroxyapatite ( $S^\circ(\text{HA})=0.92$ ) and bobierite ( $S^\circ(\text{TMPO})=1.29$ ) (Figure 8). At saturation in nesquehonite, a lower pH of 8.31 is reached, the solution being then undersaturated in brucite ( $S^\circ(\text{MH})=-0.34$ ), but still supersaturated in calcite ( $S^\circ(\text{CC})=1.01$ ), hydroxyapatite ( $S^\circ(\text{HA})=1.11$ ) and bobierite ( $S^\circ(\text{TMPO})=1.13$ ) (Figure 9).

Again, the absence of any noticeable precipitate besides nesquehonite and brucite suggests that magnesite, bobierite, calcite and hydroxyapatite cannot nucleate in DMEM, in the experimental conditions of the present study.

### Degradation mechanisms

A possible reaction scheme for the in vitro degradation of magnesium in different media, which is in line with earlier findings [29], is shown in Figure 10. It contains the often observed formation of magnesium hydroxide, but also takes into account the increased solubility of  $\text{Mg}(\text{OH})_2$  in the presence of chlorides [4]. When additional hydroxycarbonate or carbonate ions are present, as in our case due to the  $\text{CO}_2$  gassing, magnesium hydroxyl carbonate (hydrates) can be formed. It is noteworthy that we find  $\text{Mg}(\text{OH})_2$  only in the case of degradation in HBSS which has the lowest salt carbonate concentration of the tested media. Possibly, in DMEM and SBF with higher carbonate concentrations, formed  $\text{Mg}(\text{OH})_2$  is transformed (either directly or via dissolution in the presence of  $\text{Cl}^-$ ) to magnesium carbonate species. When the degradation solution contains high amounts of phosphate, as SBF, calcium phosphates may be formed which in turn may decelerate the degradation reaction. Also the presence of proteins, in our investigation modeled by the addition of FBS, will affect the degradation pathways. In addition to surface effects like the adsorption of proteins on magnesium or on degradation layers, proteins could also act directly, as some proteins are known to bind  $\text{CO}_2$  [30].

### Conclusion

This study has shown that the conditions under which the degradation of pure magnesium is investigated strongly

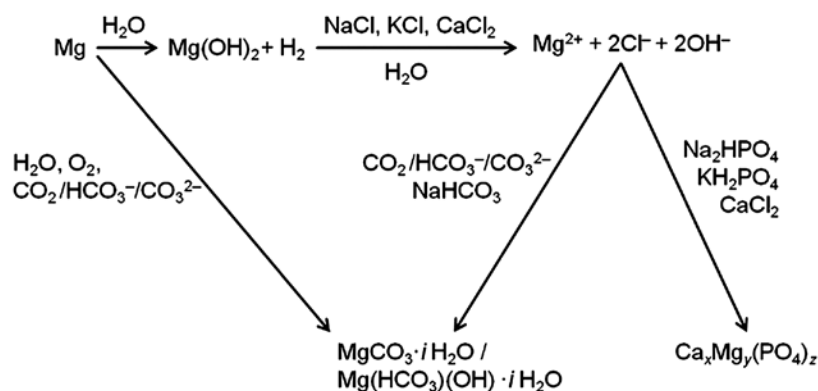


Figure 10: Proposed reaction scheme for the degradation of magnesium compounds under the examined conditions.



influence the degradation rate and the degradation products. We have chosen conditions which are close to cell-culture studies, including CO<sub>2</sub> gassing and, in part of the experiments, addition of a widely used serum-supplement containing proteins. Degradation occurred fastest in HBSS, while the supplement with proteins led to a decrease of degradation in case of HBSS and DMEM, but not in case of SBF. As expected, brucite Mg(OH)<sub>2</sub> could be found as one of the degradation products when HBSS was used. More surprisingly, nesquehonite (Mg(HCO<sub>3</sub>)(OH)·2H<sub>2</sub>O), was found to be the dominant, crystalline degradation product, formed within short terms in all media. Since it is likely that the additional carbonate source CO<sub>2</sub> promoted the formation of this magnesium hydrogen carbonate, we propose that CO<sub>2</sub> pressure ought to be taken into account in further in vitro studies. Also, the CO<sub>2</sub> pressure of the intended in vivo environment should be considered.

#### Author's statement

**Conflict of interest:** Authors state no conflict of interest.

#### Materials and methods

**Informed consent:** Informed consent has been obtained from all individuals included in this study.

**Ethical approval:** The research related to human use has been complied with all the relevant national regulations, institutional policies and in accordance the tenets of the Helsinki Declaration, and has been approved by the authors' institutional review board or equivalent committee.

## References

- Witte F. The history of biodegradable magnesium implants: a review. *Acta Biomater.* 2010;6:1680–92.
- Erne P, Schier M, Resink TJ. The road to bioabsorbable stents: reaching clinical reality? *Cardiovasc Intervent Radiol.* 2006;29:11–6.
- Waksman R, Erbel R, Di Mario C, Bartunek J, de Bruyne B, Eberli FR, et al. Early- and long-term intravascular ultrasound and angiographic findings after bioabsorbable magnesium stent implantation in human coronary arteries. *J Am Coll Cardiol Interv.* 2009;2:312–20.
- Witte F, Hort N, Vogt C, Cohen S, Willumeit R, Kainer KU, et al. Degradable biomaterials based on magnesium corrosion. *Curr Opin Solid State Mater Sci.* 2008;12:63–72.
- Witte F, Kaese V, Haferkamp H, Switzer E, Meyer-Lindenberg A, Wirth CJ, et al. In vivo corrosion of four magnesium alloys and the associated bone response. *Biomaterials.* 2005;26:3557–63.
- Janning C, Willbold E, Vogt C, Nellesen J, Meyer-Lindenberg A, Windhagen H, et al. Magnesium hydroxide temporarily enhancing osteoblast activity and decreasing the osteoclast number in peri-implant bone remodelling. *Acta Biomater.* 2010;6:1861–8.
- Xu L, Yu G, Zhang E, Pan F, Yang K. In vivo corrosion behavior of Mg-Mn-Zn alloy for bone implant application. *J Biomed Mater Res. A* 2007;83:703–11.
- Burmester A, Luthringer B, Willumeit R, Feyerabend F. Comparison of the reaction of bone-derived cells to enhanced MgCl<sub>2</sub>-salt concentrations. *Biomater.* 2014;4:e967616.
- Mueller W-D, Lucia Nascimento M, Lorenzo de Mele MF. Critical discussion of the results from different corrosion studies of Mg and Mg alloys for biomaterial applications. *Acta Biomater.* 2010;6:1749–55.
- Feyerabend F, Drücker H, Laipple D, Vogt C, Stekker M, Hort N, et al. Ion release from magnesium materials in physiological solutions under different oxygen tensions. *J Mater Sci Mater Med.* 2012;23:9–24.
- Yang L, Hort N, Willumeit R, Feyerabend F. Effects of corrosion environment and proteins on magnesium corrosion. *Corros Eng Sci Techn.* 2012;47:335–9.
- Waizy H, Weizbauer A, Modrejewski C, Witte F, Windhagen H, Lucas A, et al. In vitro corrosion of ZEK100 plates in Hank's Balanced Salt Solution. *Biomed Eng. Online* 2012;11:12.
- Fournier V, Marcus P, Olefjord I. Oxidation of magnesium. *Surf Interface Anal.* 2002;34:494–7.
- Wang Y, Wei M, Gao J, Hu J, Zhang Y. Corrosion process of pure magnesium in simulated body fluid. *Mater Lett.* 2008;62:2181–4.
- Rettig R, Virtanen S. Composition of corrosion layers on a magnesium rare-earth alloy in simulated body fluids. *J Biomed Mater Res A.* 2009;88A:359–69.
- Yamamoto A, Hiromoto S. Effect of inorganic salts, amino acids and proteins on the degradation of pure magnesium in vitro. *Mater Sci Eng.* 2009;29:1559–68.
- Tie D, Feyerabend F, Hort N, Willumeit R, Hoeche D. XPS studies of magnesium surfaces after exposure to Dulbecco's modified eagle medium, Hank's buffered salt solution, and simulated body fluid. *Adv Eng Mater.* 2010;12:B699–704.
- Bohner M, Lemaître J. Can bioactivity be tested in vitro with SBF solution? *Biomaterials* 2009;30:2175–9.
- ASTM. G31 – 72(2004) Standard Practice for Laboratory Immersion Corrosion Testing of Metals. West Conshohocken, PA: ASTM International, 2004:8.
- Abele JE. The physical background to freezing point osmometry and its medical-biological applications. *Am J Med Electron.* 1963;2:32–41.
- Prigobbe V, Mazzotti M. Precipitation of Mg-carbonates at elevated temperature and partial pressure of CO<sub>2</sub>. *Chem Eng J.* 2013;223:755–63.
- Klopprogge JT, Martens WN, Nothdurft L, Duong LV, Webb GE. Low temperature synthesis and characterization of nesquehonite. *J Mater Sci Lett.* 2003;22:825–9.
- Cheng W, Li Z. Controlled supersaturation precipitation of hydromagnesite for the MgCl<sub>2</sub>-Na<sub>2</sub>CO<sub>3</sub> system at elevated temperatures: chemical modeling and experiment. *Ind Eng Chem Res.* 2010;49:1964–74.
- Davies PJ, Bubela B. The transformation of nesquehonite into hydromagnesite. *Chem Geol.* 1973;12:289–300.
- Canterford JH, Tsambourakis G, Lambert B. Some observations on the properties of dypingite, Mg<sub>5</sub>(CO<sub>3</sub>)<sub>4</sub>(OH)·2.5H<sub>2</sub>O, and related minerals. *Mineral Mag.* 1984;48:437–42.
- dos Anjos AP, Sifeddine A, Sanders CJ, Patchineelam SR. Synthesis of magnesite at low temperature. *Carbonate Evap.* 2011;26:213–5.

27. Warren JK. Sedimentology and mineralogy of dolomitic Coorong lakes, South Australia. *J Sediment Res.* 1990; 60:843–58.
28. Shadanbaz S, Dias GJ. Calcium phosphate coatings on magnesium alloys for biomedical applications: a review. *Acta Biomater.* 2012;8:20–30.
29. Willumeit R, Fischer J, Feyerabend F, Hort N, Bismayer U, Heidrich S, et al. Chemical surface alteration of biodegradable magnesium exposed to corrosion media. *Acta Biomater.* 2011;7:2704–15.
30. Cundari TR, Wilson AK, Drummond ML, Gonzalez HE, Jorgensen KR, Payne S, et al. CO<sub>2</sub>-Formatics: how do proteins bind carbon dioxide? *J Chem Inf Model.* 2009;49:2111–5.